Eulerian Techniques for Fluid-Structure Interactions - Part II: Applications

Stefan Frei[1], Thomas Richter[1], and Thomas Wick[2]

[1] Universität Heidelberg, Institut für Angewandte Mathematik, INF 294, 69120 Heidelberg, Germany, thomas.richter@iwr.uni-heidelberg.de, stefan.frei@iwr.uni-heidelberg.de

[2] The Institute for Computational Engineering and Sciences, The University of Texas at Austin, Austin, Texas 78712, USA, twick@ices.utexas.edu

Abstract. This contribution is the second part of two papers on the Fully Eulerian formulation for fluid-structure interactions (fsi). We present different fsi applications using the Fully Eulerian scheme, where traditional interface-tracking approaches like the Arbitrary Lagrangian-Eulerian (ALE) framework show difficulties. Furthermore, we present examples where parts of the geometry undergo a large motion or deformation that might lead to contact and/or topology changes. Finally, we present an application of the scheme for growing structures. The verification of the framework is performed with mesh convergence studies and comparisons to ALE techniques.

1 Introduction

In this second part of the series on the Fully Eulerian formulation for fluid-structure interactions (fsi), we present different test-cases and applications to highlight the potential of this novel formulation. We focus on specific difficulties like large deformations, motion and contact, where interface-tracking approaches such as the Arbitrary Lagrangian Eulerian (ALE) formulation tend to fail without remeshing. Details on the derivation of the model, as well as the finite element discretization of the resulting equations are given in the first part [7].

The paper is organized as follows: In Section 2 we verify the Eulerian formulation by means of benchmark problems and comparison with ALE computations. Further, by modification of the benchmark descriptions, we go beyond the limit that can be reached by ALE techniques. Next, Section 3 presents test-cases, where the solid undergoes a very large motion. In Section 4 we focus on problems with contact and break of contact. In Section 5, we apply the locally modified finite element technique described in the first part to a simple fsi problem. Finally, in Section 6 we discuss applications with growing structures, as they appear in the growth and rupture of plaque in blood vessels. We conclude in Section 7, where we also discuss some open topics and shortcomings of the Fully Eulerian approach for fluid-structure interactions. All tests are computed either with the finite software library Gascoigne [2] or with the fsi-code [12] based on deal.II [1].

2 Numerical validation - benchmark problems

In this section, we present two test cases. The first test is based on a Computational Structure Mechanics (CSM) benchmark in which a gravitational force acts on an elastic beam deflecting it towards the bottom of the configuration (see the results in Figure 2). The second example is an extension to fluid-structure interaction. Although both tests reach a stationary limit, important issues such as interface cuts are already present. The CSM test case is split into two sub-cases. The first case is a widely used benchmark [3], in the second one we increase the force acting on the beam such that it touches the lower wall. This test case is motivated by studies of Dunne [4] and it shows the potential of the fully Eulerian formulation. The results of the first case are summarized in Table 1 (left) and compared to results obtained with an ALE code. In the second test (Wick [11]) we are able to simulate the situation where the beam touches the lower wall (up to one mesh cell because otherwise the fluid continuum equations are no longer valid), see Figure 2. For the y-displacement, the results are very similar to results obtained by Richter [9] (see Table 1 at right). For the x-displacements, we observe a slight difference, however, our findings are in reasonable agreement.

Table 1. Results for CSM 1 test in Eulerian coordinates. Force $g_s = 2ms^{-2}$ (left) and $g_s = 8ms^{-2}$ (right).

DoF	$u_x(A)[\times 10^{-3}]$	$u_y(A)[\times 10^{-3}]$
4004	−4.6371	−65.7587
12868	−8.7366	−67.5678
48768	−7.8551	−66.5940
179936	−7.0841	−66.2150
ALE	−7.1455	−65.8808

DoF	$u_x(A)[\times 10^{-3}]$	$u_y(A)[\times 10^{-3}]$
20988	−25.26	−192.61
54744	−54.55	−195.26
184629	−53.33	−196.11
691233	−55.04	−196.89
(ref. [9])	−66.857	−192.35

Table 2. Results for the FSI 1 benchmark.

Level	DoF	$u_x(A)[\times 10^{-3}]$	$u_y(A)[\times 10^{-3}]$	Drag	Lift
3	131976	0.0236	0.8146	18.831	0.7784
	(ref. [8])	0.0227	0.8209	14.295	0.7638

In the second test, the FSI 1 benchmark [3] is considered in which a parabolic inflow is prescribed. The elastic beam deforms caused by a pressure difference because of the non-symmetric location of the cylinder. First results using a stationary code were presented in [10]. Now, we use our recent advances [9, 11] to recompute this example with a nonstationary code version. Our findings are summarized in Table 2. In order to keep the computational cost reasonable, local mesh refinement around the elastic beam is applied.

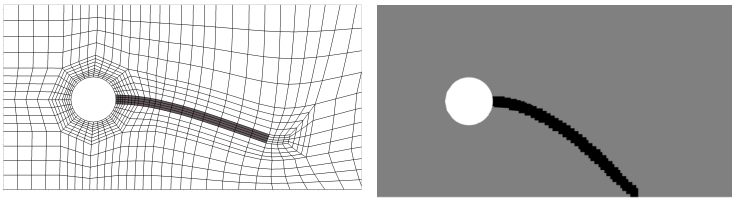

Fig. 1. CSM-1 benchmark test (left) and CSM touching the lower wall for $g_s = 8ms^{-2}$ (right). The left figure displays the ALE computation with the moving mesh whereas the right shows the Eulerian result.

3 Large motion - 360^o rotation

Usually, the reason for the break-down of the ALE approach is loss of regularity in the ALE transformation map and not the large deformation or motion of the structure itself.

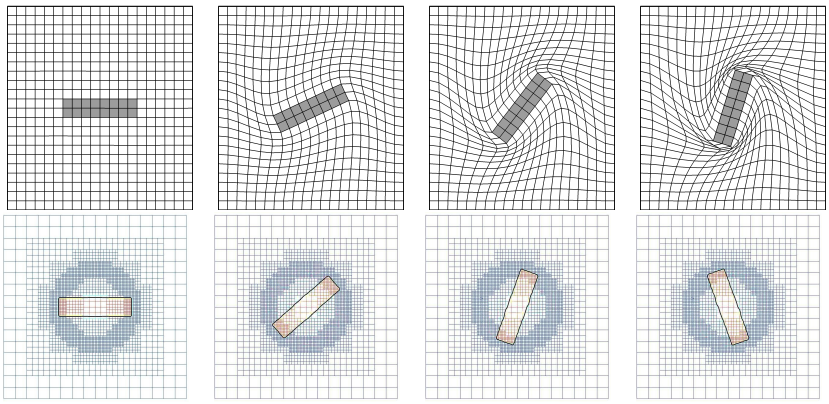

Fig. 2. Rotational flow around an unmounted obstacle at different time steps. Top row: ALE computation. Bottom row: Fully Eulerian.

In Figure 2, we show a prototypical configuration: an (elastic or rigid) body $\mathcal{S} = \mathcal{S}(0)$ is centered in a flow container $\mathcal{S} \subset \Omega$. By a rotational flow in the fluid-domain $\mathcal{F} = \mathcal{F}(0) = \Omega \setminus \mathcal{S}(0)$ the object starts to rotate. Here, it is not a deformation of the solid but a rigid body rotation that causes severe problems in ALE computations (top line of Figure 2).

In the Fully Eulerian formulation, the large motion and rotation does not cause any problems, as the fluid problem is given in the Eulerian framework, see the bottom line of Figure 2. In this framework, the interface moves through the domain and must be captured by the Initial Point Set. As these

computations have been done without a specially fitted interface finite element method, we observe a strong loss of accuracy. For the Eulerian framework, meshes with a finer resolution are required to reach the same accuracy as with an ALE approach. In order to obtain approximately the same accuracy, we used about 4 000 locally refined elements for the Eulerian approach vs. 400 elements in the ALE case (cf. Figure 2) .

As an interface-capturing technique, the Fully Eulerian approach is not strictly mass-conserving, the solid mass

$$m_s(u) = \int_{\mathcal{S}(t)} J(u)\rho_s^0 \,\mathrm{d}x$$

depends on the accuracy of the captured interface. For this test-case, we observe, that linear finite elements (even without fitted interface modifications) show second order in capturing the solid mass

$$|m_s(u) - m_s(u_h)| = O(h^2).$$

4 Touching the boundary

We consider a test problem, that has been introduced in [9]. An elastic ball "falls" due to gravity in a viscous fluid until it touches the bottom of the rigid fluid domain. Due to elasticity, the ball bounces off and is elevated, then falls down again for several times until the motion is finally damped by viscous effects.

The fixed computational domain is set to $\Omega = (-1,1)^2 m$, and at reference time $t = 0$ the system is at rest, with the ball being centered in the origin $\mathcal{S}(0) = \{x \in \Omega : \ |x| < 0.4m\}$. The fluid-domain $\mathcal{F}(0) = \Omega \setminus \mathcal{S}(0)$ is governed by a viscous incompressible Navier-Stokes fluid with density $\rho_f = 10^3 kgm^{-3}$ and kinematic viscosity $\nu_f = 10^{-2}m^2s^{-1}$. The elastic ball has density $\rho_s^0 = 10^3 kgm^{-3}$ and the Lamé coefficients $\mu_s = 10^4 kg\, m^{-1}s^{-2}$ and $\lambda_s = 4 \cdot 10^4 kg\, m^{-1}s^{-2}$. The problem is driven by a right hand side, that acts on the solid-domain only, $\mathbf{f}_s = -1ms^{-2}$ and $\mathbf{f}_f = 0$. On the bottom part of the boundary $\Gamma_{\mathrm{bot}} = \{(-1,1) \times \{-1\}\}$ we prescribe homogenous Dirichlet conditions for the velocities $\mathbf{v} = 0$. On all other parts of the boundary $\partial\Omega \setminus \Gamma_{\mathrm{bot}}$ we prescribe the "do-nothing" outflow condition for the fluid $-p_f\mathbf{n} + \rho_f\nu_f\partial_n\mathbf{v}_f = 0$. Finally, we prescribe homogenous Neumann conditions for the displacement $\partial_n\mathbf{u} = 0$ on the complete boundary $\partial\Omega$.

The main interest of this test case is the contact of the structure with the boundary of the domain. In Figure 3, we plot the distance of the ball to the ground. First we observe, that the ball touches the ground for a short time-interval and then bounces off. The maximum elevation is reduced after each contact with the domain's boundary. Further, we show the normal wall stress on the lower boundary and the norm of the Cauchy stresses within the

solid:

$$J_{\text{wall-stress}} = \int_{\Gamma_{\text{bot}}} \mathbf{n} \cdot \boldsymbol{\sigma}_f \mathbf{n} \, \mathrm{d}o, \quad J_{\text{solid-stress}} = \int_{\mathcal{S}(t)} \boldsymbol{\sigma}_s : \boldsymbol{\sigma}_s \, \mathrm{d}x.$$

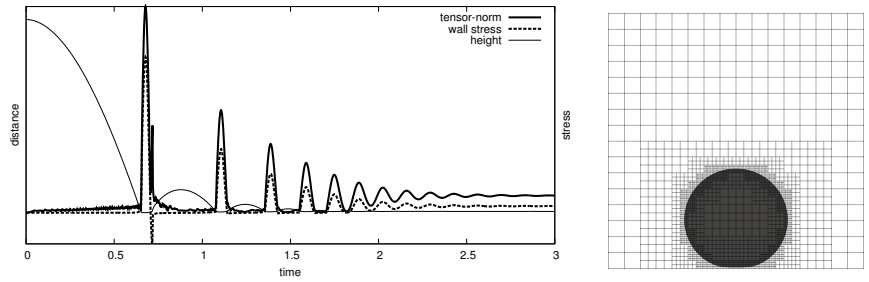

Fig. 3. Left: height of the falling ball over the ground, wall-stress and solid Cauchy stress. Right: configuration at the time of closest contact $t = 0.675$. Small undershoots in the wall-stress are due to the forces of the incompressible fluid on the boundary at separation time.

There will always be a thin layer of fluid around the structure, such that there is no real "contact" between both phases. The right part in Figure 3 shows a plot of the elastic ball on the fixed background mesh at the time where ball and boundary are closest. The forces are transferred via the remaining small layer of fluid. These results are stable under refinement of the temporal and spatial discretization. It however still remains to show, that the realization of contact, which is modeled by the discretization only, gives realistic results. Here, comparisons to experiments and numerical benchmarking with alternative formulations are necessary steps in future work.

5 Locally modified finite element scheme

In this section, we present first nonstationary results using the Locally Modified Finite Element scheme described in the first part [5, 7] applied to a simplified fluid-structure interaction problem. The problem under consideration consists of an elastic ball in the middle of a fluid governed by the linear Stokes equation. The elastic solid is governed by a fully linearized elasticity model. The flow field is driven by a prescribed parabolic inflow on the left-hand side of the domain. This causes the elastic ball to move towards the right side where we prescribe the do-nothing outflow condition. In Figure 4, we show screen-shots of simulation results at four different time steps. The time step was chosen $k = 10^{-3}$.

As described in [5, 7], we use a fixed patch mesh for all time steps. Outside the interface region, we split each patch $P \in \Omega_h$ into four quadrilaterals (type 1). Patches cut by the interface are split into eight triangles that resolve the

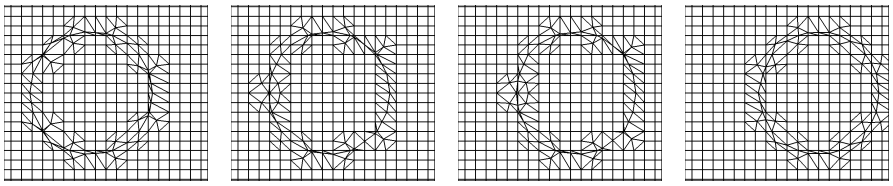

Fig. 4. Screen-shots of a moving elastic ball simulated using the Locally Modified Finite Element scheme at time $T = 0.05$, $T = 0.1$, $T = 0.15$ and $T = 0.2$.

interface with a linear approximation (types 2 to 4). The type assigned to a patch may vary in every time step depending on the position of the interface. Although the aspect ratio of the triangles can get arbitrarily bad, we can make sure, that all triangles have interior angles bound away from π. This guarantees robust interpolation estimates. To cope with the bad conditioning of the system matrix, we use a hierarchical basis on those patches, that are cut by the interface.

This approach is equivalent to a fitted finite element method using a mixed triangular-quadrilateral mesh, which is well known to give optimal approximation properties. However, instead of modifying the mesh, we locally modify the finite element basis. The number of unknowns and the connectivity of the system matrix does not depend on the interface location.

6 Growing structures and clogging phenomena

In this final example, we present results showing our recent efforts in modeling and simulating growing solids and clogging phenomena. The key idea relies on a multiplicative decomposition of the displacement gradient into an elastic and a growth part. The fundamental relation (see Part I [7]) is given by

$$F = \hat{F}^{-1}. \tag{1}$$

Now, the Eulerian displacement gradient is split into a growth part and an elastic part using relation (1):

$$F = \hat{F}^{-1} = \hat{F}_g^{-1}\hat{F}_e^{-1} =: \hat{F}_g^{-1}F_e, \quad F_e := \hat{F}_e^{-1},$$

and

$$J := \hat{J}^{-1} = \hat{J}_g^{-1}\hat{J}_e^{-1} =: \hat{J}_g^{-1}J_e, \quad J_e := \det F_e = \hat{J}_e^{-1}.$$

The growth tensor is defined as $\hat{F}_g^{-1} := \hat{g}(\hat{x}, t)I$.

The problem is driven by a pressure difference described as cosine function and simultaneously by growth of the structure. Consequently, we consider two effects, namely, fsi-interaction and solid-growth. The configuration and the material parameters are taken from [6], Example 2. In addition to these tests,

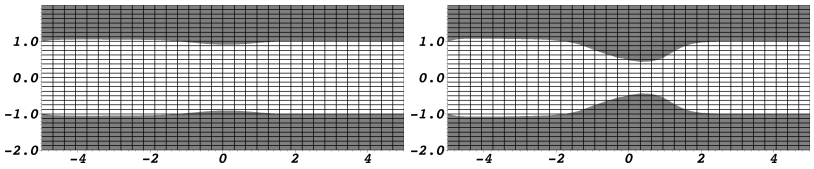

Fig. 5. Configuration 2: Deformation at times $T = 10, 40$ in the time interval $[0, 80]$.

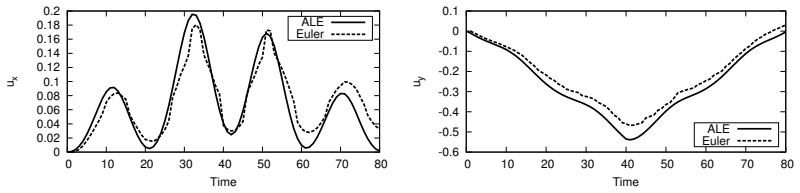

Fig. 6. Deformation of the top solid at channel's mid-point at times $T = 10, 40$ in the time interval $[0, 80]$.

we now consider growth and back-growth of the solid (for instance when a plaque-disease occurs and vanishes after treatment). By observing Figure 5 and Figure 6, we see that the findings in both frameworks show similar qualitative behavior. The results of the Eulerian approach are less accurate and stable, as this test-case is computed using the standard non-fitted finite element approach without the modifications described in Section 5.

7 Conclusion

As shown in our studies, the Fully Eulerian formulation for fluid-structure interactions offers an alternative modeling approach, that can be preferable for certain classes of problems. As a monolithic model, one can use strong implicit discretization schemes with large time-steps, independent of the problem's stiffness. One benefit of the Eulerian scheme is the simple incorporation of complex models, like, e.g. active growing solids. As a drawback, we point out the interface-capturing type of this approach. To achieve good approximation at the interface, additional computational effort is required. Often, finer meshes are required, however, the Fully Eulerian approach will not fail, if motion of the solid gets large. The full use of the locally modified finite elemente scheme [5, 7] for nonstationary problems will essentially remove this drawbacks. Among the large variety of different schemes for fluid-structure interactions that are able to deal with large deformation and motion, the peculiarity of the Fully Eulerian approach is its strictly monolithic character. If implicit discretization schemes and solvers are desirable or if adjoint schemes for error estimation or optimization are to be used, the Eulerian scheme can be easily embedded into the usual variational framework.

Bibliography

[1] W. Bangerth, R. Hartmann, and G. Kanschat, *deal.II – a general purpose object oriented finite element library*, ACM Trans. Math. Softw. **33**:4 (2007), 24/1–24/27.

[2] R. Becker, M. Braack, D. Meidner, T. Richter, and B. Vexler, *The finite element toolkit* Gascoigne, http://www.gascoigne.uni-hd.de.

[3] H.-J. Bungartz and M. Schäfer, *Fluid-structure interaction: Modelling, simulation, optimization*, Lecture Notes in Computational Science and Engineering, vol. 53, Springer, 2006.

[4] T. Dunne, *An eulerian approach to fluid-structure interaction and goal-oriented mesh refinement*, Int. J. Numer. Math. Fluids. **51** (2006), 1017–1039.

[5] S. Frei and T. Richter, *A locally modified parametric finite element method for interface problems*, SIAM J. Numer. Anal. (submitted, 2013).

[6] S. Frei, T. Richter, and T. Wick, *Solid growth and closure in fluid-structure interaction computed in ALE and fully Eulerian coordinates*, in preparation, 2013.

[7] ———, *Eulerian Techniques for Fluid-Structure Interactions - Part I: Modeling and Simulation*, ENUMATH 2013 Proceedings, Lecture notes in computational science and engineering, vol. ., Springer, 2014.

[8] J. Hron and S. Turek, Proposal for numerical benchmarking of fluid-structure interaction between an elastic object and laminar incompressible flow, vol. 53, 146 – 170, Springer-Verlag, 2006, pp. 146 – 170.

[9] T. Richter, *A fully eulerian formulation for fluid-structure-interaction problems*, J. Comp. Phys. **233** (2013), 227–240.

[10] T. Richter and T. Wick, *Finite elements for fluid-structure interaction in ale and fully eulerian coordinates*, Comput. Methods Appl. Mech. Engrg. **199** (2010), 2633–2642.

[11] T. Wick, *Fully Eulerian fluid-structure interaction for time-dependent problems*, Comput. Methods Appl. Mech. Engrg. **255** (2013), 14–26.

[12] ———, *Solving monolithic fluid-structure interaction problems in arbitrary Lagrangian Eulerian coordinates with the deal.ii library*, Archive of Numerical Software **1** (2013), 1–19.